# Ultrasensitive electrochemical sensing platform based on graphene wrapping $SnO_2$ nanocorals and autonomous cascade DNA duplication strategy

Ying-Xu Chen, Ke-Jing Huang, Feng Lin, Lin-Xia Fang


www.elsevier.com/locate/talanta

PII: S0039-9140(17)30760-9
DOI: http://dx.doi.org/10.1016/j.talanta.2017.07.042
Reference: TAL17741

To appear in: *Talanta*

Received date: 26 May 2017
Revised date: 12 July 2017
Accepted date: 13 July 2017

Cite this article as: Ying-Xu Chen, Ke-Jing Huang, Feng Lin and Lin-Xia Fang Ultrasensitive electrochemical sensing platform based on graphene wrapping $SnO_2$ nanocorals and autonomous cascade DNA duplication strategy, *Talanta* http://dx.doi.org/10.1016/j.talanta.2017.07.042

# Ultrasensitive electrochemical sensing platform based on graphene wrapping $SnO_2$ nanocorals and autonomous cascade DNA duplication strategy

Ying-Xu Chen [a,b,c], Ke-Jing Huang [a,b,c,*], Feng Lin [a,b,c], Lin-Xia Fang [a,b,c]

[a] *College of Chemistry and Chemical Engineering, Xinyang Normal University, Xinyang 464000, China*

[b] *Henan Province Key Laboratory of Utilization of Non-metallic Mineral in the South of Henan, inyang Normal University, Xinyang 464000, China*

[c] *Institute for Conservation and Utilization of Agro-bioresources in Dabie Mountains, Xinyang Normal University, Xinyang 464000, China*

[*]Corresponding author. Tel.: +86 376 6390611; fax: +86 376 6390611. E-mail address: kejinghuang11@163.com (K.-J. Huang)

**ABSTRACT:** In this work, a sensitive, universal and reusable electrochemical biosensor based on stannic oxide nanocorals-graphene hybrids ($SnO_2$ NCs-Gr) is developed for target DNA detection by using two kinds of DNAenzymes for signal amplification through an autonomous cascade DNA duplication strategy. A hairpin probe is designed composing of a projecting part at the 3′-end as identification sequence for target, a recognition site for nicking endonuclease, and an 18-carbon shim to stop polymerization process. The designed DNA duplication–incision–replacement process is handled by KF polymerase and endonuclease, then combining with gold nanoparticles as signal carrier for further signal amplification. In the detection system, the electrochemical–chemical–chemical procedure, which uses ferrocene methanol, tris(2-carboxyethyl)phosphine and L-ascorbic acid 2-phosphate as oxidoreduction neurogen, deoxidizer and zymolyte, separately, is applied to amplify detection signal. Benefiting from the multiple signal amplification mechanism, the proposed sensor reveals a good linear connection between the peak current and logarithm of analyte concentration in range of 0.0001-$1\times10^{-11}$ mol $L^{-1}$ with a detection limit of $1.25\times10^{-17}$ mol $L^{-1}$ (S/N=3). This assay also opens one promising strategy for ultrasensitive determination of other biological molecules for bioanalysis and biomedicine diagnostics.

Graphical abstract

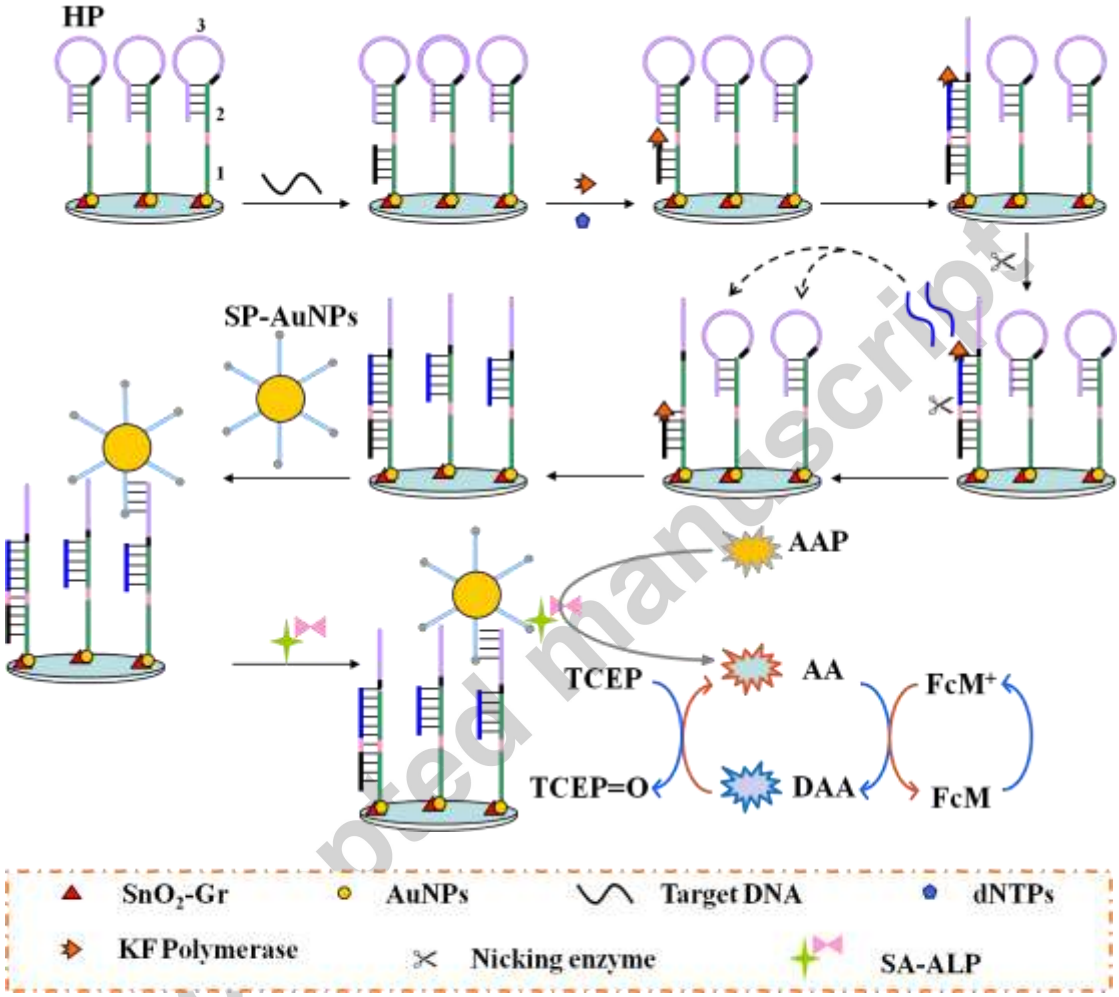




A signal-amplification biosensor is developed based on $SnO_2$ NCs-Gr hybrids and autonomous cascade DNA replication strategy for DNA detection.

**Keywords:** Stannic oxide nanocorals-graphene hybrids; Autonomous cascade DNA duplication strategy; Endonuclease; Polymerase; Signal amplification



## 1. Introduction

The ultrasensitive detection of DNA sequences affords significant information for food quality inspection, clinical research, and forensic medical appraisal [1]. Electrochemical methods are simple, rapid and sensitive [2-7] and widely used for DNA detection. So far, multifarious signal amplification technologies have been applied in electrochemical DNA sensors [8]. For example, polymerase chain reaction (PCR) has an evident advantage in sensitivity but the demands of accurate temperature control and rigorous trained analysts also exposes limitations on the wide

application of PCR [9]. Rolling circle amplification (RCA), in contrast, is an isothermal enzymatic DNA duplication process, which is easier and more convenient than PCR. However, the amplification potency of RCA is less than that of PCR [10]. Although the catalyzed hairpin assembly (CHA) amplification strategy couples with target recycling and post-amplification is popular now [11], it is usually restrained by the comparatively rigor and intricacy design principle for the adoptive hairpin DNA. Thus, the desire to develop the highly sensitive, low-complexity and convenient methods for the specific and sensitive detection of DNA is rather intense.

For sensitive detection of DNA, nanomaterials are usually used because they have high specific surface area, preeminent electro-conductivity and excellent biological compatibility [12]. Graphene (Gr), a typical two-dimension nanomaterial, has many favourable physicochemical properties. It has been revealed numerous hopeful applications in electrochemical biosensors [13-15]. Stannic oxide ($SnO_2$) crystals attract considerable attentions due to their fascinating physical and chemical properties. They have been widely applied in immunosensor [16], photocatalysis [17], lithium batteries [18] and gas sensors [19] due to advantages of low cost, good biological compatibility, abundant sources and simple synthetic process. Intriguingly, it's well-grounded that the geometric shape and surface characteristics can markedly affect the physiochemical properties of metal oxides. The controlled anisotropic morphologies such as nanorods, nanowires and nanosheets are looking forward to improve electrochemical performance of metal oxides over their particle-like counterparts [20,21]. Therefore, highly ordered nanostructures by *in situ* preparation

may open up the complete application potential of Gr based hybrids. Based on this, we recommend a synthetic strategy to structure coral-like $SnO_2$ embellished Gr nanosheets for biosensor. With the selective nucleation of $SnO_2$ nanocorals (NCs) insetting into Gr sheets, the obtained nano-structures can be used as electrode substrate with high mobility of conducting electrons [22].

Recently, it is reported that the autonomous duplication–incision–replacement strategy by using polymerase and nicking endonuclease owns an important hope to replace PCR because of its easy manipulation, superior selectivity and good sensitivity [23-25]. In this work, an autonomous cascade DNA duplication tactic is efficaciously combined with enzyme, $SnO_2$ NCs-Gr hybrids and an electrochemical–chemical–chemical (ECC) redox cycling system post-amplification tactic to structure an ultrasensitive electrochemical DNA biosensor. Gold nanoparticles (AuNPs) are used as signal carrier. The elaborate design of hairpin DNA probe (HP) is composed of a ledge at 3′-end, a recognition site and an alkane shim. Their functions are used to recognize targets and stop the polymerization reaction. The spontaneous DNA duplication–incision–replacement pattern is handled by Nb.BbvCI endonuclease and KF polymerase. AuNPs loaded enzyme is introduced for signal readout. This kind of DNA detection strategy is conducted by Nb.BbvCI endonuclease and KF polymerase, which is aim to recycle DNA snippet to release the loop of HP to gain the ends of signal amplification, manifesting that it is good for the assembly of the reborn biosensor. ECC redox cycling is also used for signal amplification. Overall, the current strategy makes a valid jointing for the target DNA and proceeds the signal

amplification by duplication and incision, therefore gives rise to an momentous chance for the nucleic acid biosensor with satisfactory performance.

## 2. Experimental

### 2.1. Reagents

Klenow Fragment polymerase (KF polymerase), streptavidin-conjugated alkaline phosphatase (SA-ALP), deoxyribonucleoside triphosphates (dNTPs) tris(carboxyethyl)phosphine (TCEP), Nb.BbvCI endonuclease, L-ascorbic acid 2-phosphate (AAP) and ferrocene methanol (FcM) were obtained from Sigma–Aldrich (Shanghai, China). DNA sequences were prepared from Sangon Biotech. Co., Ltd. (Shanghai, China) and their sequences were as follows:

HP:

5’-GTGTAATGGGCGCACCTCTTTTTTTT-shim18-GAGGTGCGCCCATTACACTGTTCAGCCCTCAGCATCTATACAACCTACTACCTAATTTTT$(CH_2)_3$-SH-3’

SP: 5’-Biotin-GAGGTGCGCCCATTACACTTTTT-$(CH_2)_3$-SH-3’

Target sequence: 5’-TTAGGTAGTAGGTTGTATAGAT-3’

Single-base mismatched sequence: 5’-TTAGGTAGTAGGTTGTATAGCT-3’

Three-base mismatched sequence: 5’-TTAGGTAGTAGGTTGTATGGCT-3’

Non-complementary target: 5’-GAACAGTTCACGATCTGGACCA-3’

### 2.2. Apparatus

Electrochemical detection was performed on CHI 660E electrochemical workstation (CH Instruments, Shanghai, China). Hitachi S-4800 scanning electron microscope (Tokyo, Japan) and JEM 2100 transmission electron microscope (JEOL, Tokyo, Japan) were applied for the morphological characterizations. A model D/max-rA diffractometer (Rigaku, Tokyo, Japan) was used to record X-ray diffraction (XRD) data. The particle size was detected on Malvern Zetasizer 3000 HS (Malvern Instruments, Worcestershire, UK).

### 2.3. Preparation of $SnO_2$ NCs-Gr

The graphene oxide (GO) was first prepared by the modified Hummers' method [26]. The GO was then uniformly dispersed in water and subsequently mixed with $NaBH_4$. The mixture was thermally treated at 95 °C for 24 h. After that, Gr was obtained after washed with water and dried at 60 °C. For the synthesis of $SnO_2$ NCs-Gr, graphene sheets (7.5 mg), $SnCl_4 \cdot 5H_2O$ (0.1 M) and NaOH (1.2 M) were first dissolved in deionized water (15 mL). Then, the mixture was treated with sonication (300 W) for 2 h, and then hydrothermal synthesis was performed at 220 °C for 24 h. Finally, the product was annealed at 600 °C in a $N_2$ flow for 3 h.

### 2.4. Preparation of biotin-tagged signal probe bonding AuNPs

The preparation of AuNPs was consulted according to reference [27]. 100 mL 0.01% $HAuCl_4$ solution was boiled with energetic stirring. Then 2.5 mL 1% sodium

citrate solution was fast added. When the color turned amaranth, the solution was cooled to room temperature and then reserved in a brown reagent bottle at 4 °C.

The signal probe DNA (SP DNA) bonding AuNPs (SP-AuNPs) was prepared as follows [28]: 50 μL biotin-labled SP (10 μM) was added to freshly prepared AuNPs (1 mL) and incubated for 20 h at 37 °C. Afterward, 0.1 mL PBS (pH 7.4) containing 2.0 M sodium chloride was dropwised. Then the red precipitate was collected and washed with PBS for three times. The obtained SP-AuNPs was finally stored at 4 °C.

**2.5. Fabrication of DNA biosensor**

Prior to modification, 1.0 mg $SnO_2$ NCs-Gr hybrids were dissolved in 1.0 mL distilled water. The surface of the GCE was polished to a mirror-like smooth by alumina slurry. After washed and dried with nitrogen gas, 8 μL $SnO_2$ NCs-Gr was dropped onto the preprocessed electrode to get $SnO_2$-Gr/GCE. Then AuNPs were coated on $SnO_2$-Gr/GCE by electrochemical deposition in 0.1% $HAuCl_4$ containing 0.1 M $KNO_3$ for 40s. Thereafter, 8 μL 10 mM Tris–HCl ($1.0\times10^{-2}$ mol $L^{-1}$ TCEP, 0.5 mol $L^{-1}$ NaCl, pH 7.4) containing $5.0\times10^{-4}$ mol $L^{-1}$ HP was covalently immobilized on AuNPs/$SnO_2$ NCs-Gr/GCE by incubation for overnight. Then, the electrode was dipped in 0.5 mM MCH for 1 h, and then incubated in 50 μL 20 mM Tris-HCl buffer (0.14 mol $L^{-1}$ NaCl, $5.0\times10^{-3}$ mol $L^{-1}$ $MgCl_2$) including 8 U Nb.BbvCI endonuclease, 8 U KF polymerase, 0.8 mM dNTPs and various levels of target for 2 h at 37 °C. After washed with 10 mM Tris–HCl buffer, the electrode was immersed in 50 μL SP-AuNPs for 2 h. For decreasing adsorption of the bio-enzyme and improving the

reproducibility, 1.0 mg $mL^{-1}$ BSA solution was applied on the electrode. Finally, 10 μL SA-ALP (10 mg $mL^{-1}$) was dropped on electrode and incubated at 37 °C for 40 min.

### 2.6. Electrochemical measurements

Before electrochemical measurement, the biosensor was incubated in 20 mL Tris ($1.0\times10^{-2}$ mol $L^{-1}$, pH 8.0) containing $5.0\times10^{-2}$ mol $L^{-1}$ AAP and 1 mM $MgCl_2$ for 30 min. Thereafter, the DPV curves were recorded in Tris buffer containning 0.5 mM TCEP and 0.2 mM FcM. The pulse amplitude was 0.005 V and pulse width was 0.05 s. Impedance experiments were recorded in $1.0\times10^{-3}$ mol $L^{-1}$ potassium ferricyanide containing 0.1 mol $L^{-1}$ potassium chloride in the range of 0.1-100 kHz.

## 3. Results and discussion

### 3.1. Biosensor design

The fabrication process of proposed biosensor was schematically demonstrated in Scheme 1. Our biosensor is composed of a hairpin probe DNA (HP), Nb.BbvCI endonuclease, KF polymerase and biotin-tagged signal probe DNA bonding AuNPs. The sulfhydryl-labeled HP at 3'-end immobilized on the AuNPs/$SnO_2$ NCs-Gr/GCE forms a hairpin probe, which can be divided into three parts and named as part 1, 2 and 3. Part 1 is applied as the recognition segment. Part 3 (the purple area of HP in Scheme 1) is the sequences that is complementary to part 2. A carbon shim (the black area of HP in Scheme 1) is intercalated between part 2 and 3 to stop polymerization

process. The sequence between part 1 and 2 (the pink area of HP in Scheme 1) can be regarded as the recognition site for Nb.BbvCI endonuclease. When target DNA exists, it hybridizes with part 1 of HP and starts polymerization process from the 3′-end of target under existence of KF polymerase and dNTPs. This polymerization reaction creates a replicate through segmental HP snippet covering Nb.BbvCI recognition site and part 2. In this place, 18-carbon shim can terminate the polymerization process in the tail of part 2 undisputedly. Simultaneously, the hairpin-like probe DNA can be unfolded when the polymerization reaction happens and part II is separated with part 3. During the polymerization reaction, the new fruiting recognition site for Nb.BbvCI nicking endonuclease triggers one autonomous duplication–incision–replacement reaction, hence produces plentiful single-stranded DNA (ssDNA) snippet [29,30]. These new ssDNA snippets (the blue wave in Scheme 1) could be regarded as new like-target to hybridize with part 2 of HP and unfold more new HPs to release part 3. Afterwards, the unbridled part 3 of HP is hybridized with SP DNA, so that the biotin labeled SP DNA bonding AuNPs (SP-AuNPs) can be immobilized on the part 3 of HP for further signal amplification. The SP-AuNPs is applied as signal carrier ascribing to binding a large amount of SP for each gold nanoparticle. Obviously, SP-AuNPs is hardly hybridized with the original HP because of the looping function of complementary part in HP's 5′-end. Therefore, once part 3 of HP is revealed from its loop, the SP-AuNPs are linked on the 5′-end of HP. The SA-ALP can be combined with biotin by the specific affinity reaction. In the detection system, the enzymatic products triggered the ECC redox circulation. AAP, FcM and TCEP are applied as

enzyme substrate, redox mediator and deoxidizer, respectively. Specifically, AAP is a first-rank substrate for ALP during detection process due to intrinsic property [31]. Ferrocene ramification is relatively stable in air and AA accelerated the reproduction of FcM result in an increase of FcM during the electrochemical scanning [32,33]. While TCEP is used as a stabilized and suitable chemical deoxidizer to regenerate AA from dehydroascorbic acid (DAA, its oxidation product), therefore forming the signal amplification [31,34]. When there is no target, HP cannot be opened and KF polymerase cannot work in target. In current strategy, the autonomous DNA duplication–incision–replacement reaction proceeds by KF polymerase and nicking endonuclease, contributing to final ECC detection system, thus supplies a precise detection toward target DNA. In addition, the proposed sensor can be easily applied into other DNA sequences by only simply replacing the recognition sequence of HP.

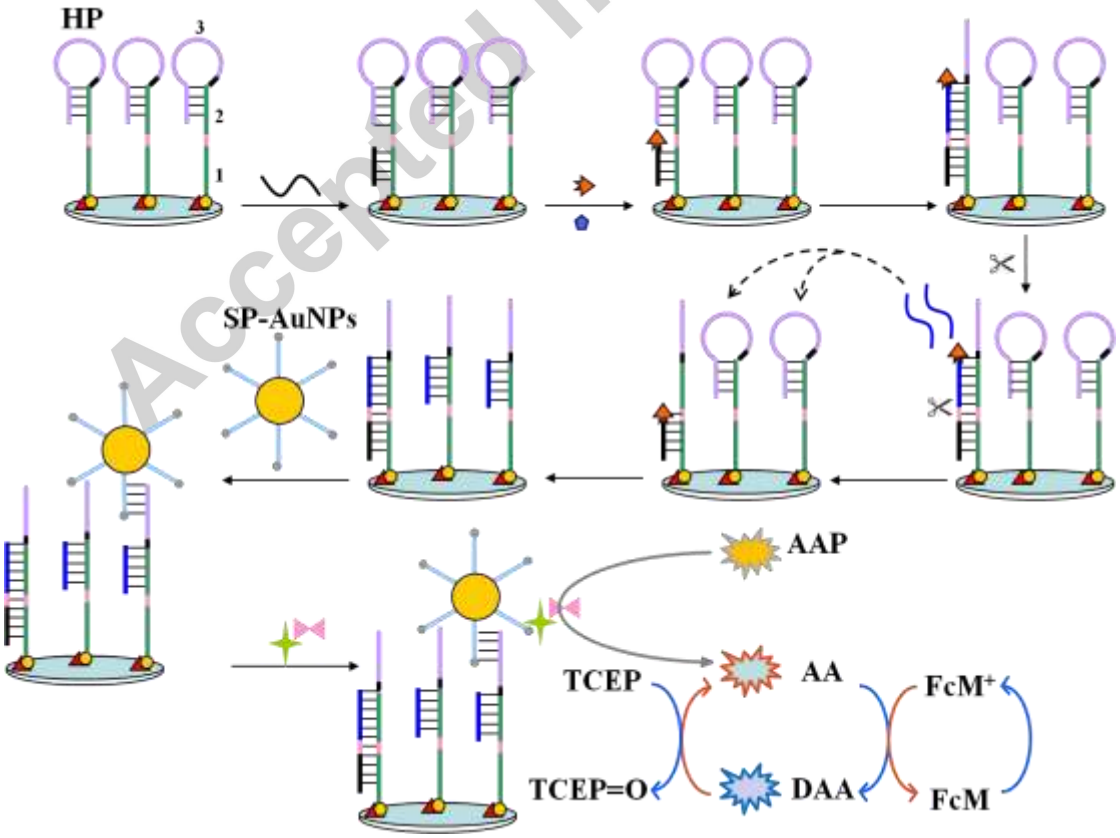


**Scheme 1** The schematic for target determination with $SnO_2$ NCs-Gr hybrids coupling with DNAenzyme for signal amplification strategy.

### 3.2. Characterization of $SnO_2$ NCs-Gr composites

The structural and morphological details of the as-prepared $SnO_2$ NCs-Gr hybrids were examined by SEM and TEM. SEM image (Fig. 1A) shows $SnO_2$ nanorods are assembling into a coral. The green oval part in Fig. 1A indicates some $SnO_2$ nanocorals are covered by Gr partially. Fig. 1B is the magnifying image of Fig. 1A and it displays coral-like $SnO_2$ nanorods. The figure also shows these $SnO_2$ NCs are trapped and segregated by Gr sheets.

The low-magnification TEM image exhibits individual $SnO_2$ nanorod in the coral assembly, which is partially wrapped by Gr sheets with thicknesses of a few layers (Fig. 1C). The diameter of the nanorods is determined to be about 100 nm. The high-magnification TEM images (Fig. 1D and 1E) denote two sets of dominant crystal lattices in the nanorods with respective interfringe spacing of 0.33 and 0.26 nm, corresponding to the (110) and (101) facets of tetragonal rutile $SnO_2$. It is confirmed that the anisotropic growth along the c-axis is thermodynamically preferred, since the surface energy of (001) plane is the highest one [35].

Fig. 1F shows the typical XRD data of the prepared $SnO_2$ NCs-Gr hybrids, clearly suggesting the tetragonal cassiterite construction (JCPDS no. 41-1445). The

broadened peaks indicate the formation of $SnO_2$ NCs, but the diffraction signal of Gr in the hybrids is weak and indistinguishable, which might be put down due to below reasons: (1) the unordered interface of construction generated by interface of incorporation between $SnO_2$ NCs and Gr [36]; (2) disordered stacking nature of Gr in the compound [37].

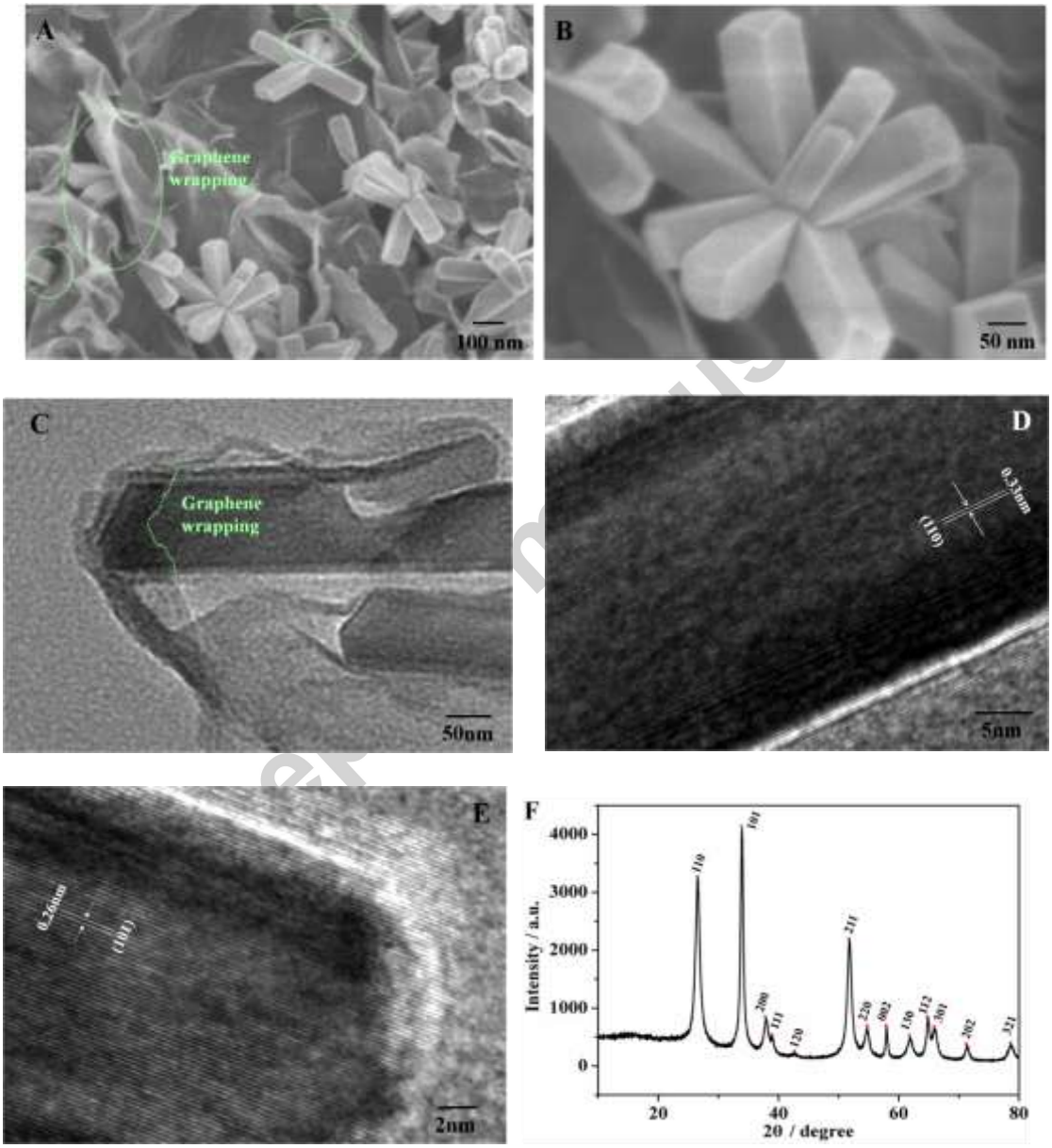


**Fig. 1** SEM images of $SnO_2$ NCs-Gr hybrids (A, B); TEM image of $SnO_2$ NCs-Gr hybrids (C); High-magnification TEM images of $SnO_2$ nanorods (D, E); XRD patterns

of $SnO_2$NCs-Gr hybrids (F).

### 3.3. Characterization of AuNPs and SP-AuNPs

The prepared AuNPs and SP-AuNPs are studied by TEM (Fig. 2A and 2B). There is no distinct variation in morphology between SP-AuNPs and AuNPs. The sizes of both products were further studied by DLS techniques (Fig. 2C and 2D). The average dynamic size for SP-AuNPs clearly enlarged than AuNPs. The enlarged size comes from the bonding SP [23,38]. Moreover, it can be seen from UV–vis spectra (Fig. 2E) that the typical absorption peak of AuNPs changes from 521 to 525 nm because of the ornament of SP DNA on AuNPs [39].

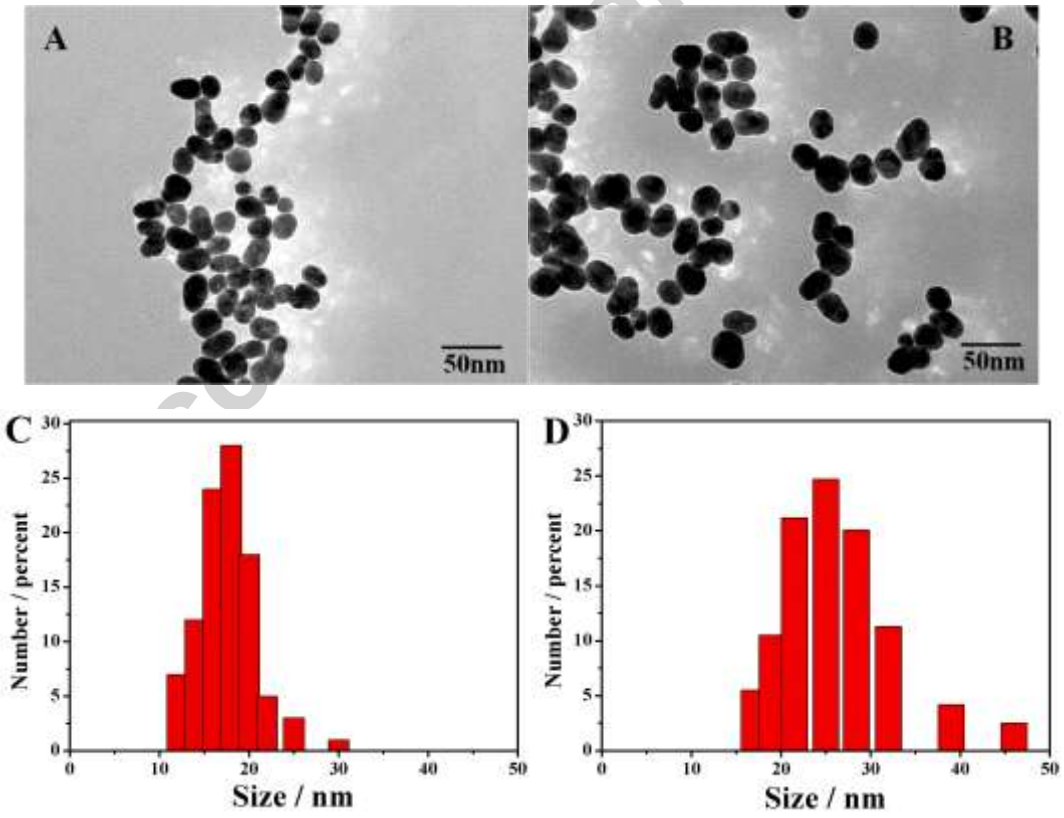

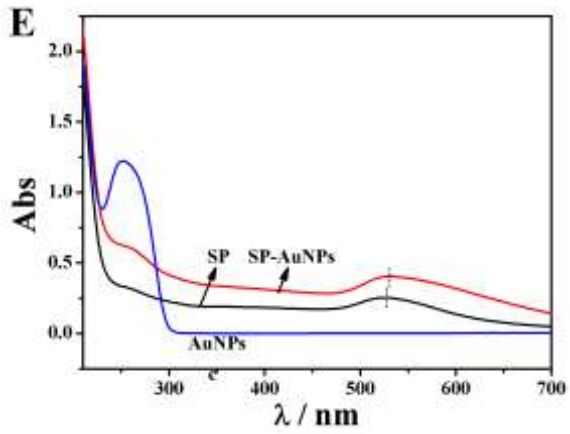


**Fig. 2** TEM of AuNPs (A) and SP-AuNPs (B); DLS of AuNPs (C) and SP-AuNPs (D); (E) UV-vis of AuNPs, SP and SP-AuNPs.

### 3.4. Electrochemical characterization

Electrochemical characterization of different electrodes was studied by CV in 1.0 mmol $L^{-1}$ potassium ferricyanide containing 0.1 mol $L^{-1}$ KCl (Fig. 3A). It exhibits a couple of redox peaks on bare GCE (curve a), which is consistent with invertible redox reaction of potassium ferricyanide. For $SnO_2$ NCs-Gr modified GCE, the peak current enhances greatly since $SnO_2$ NCs-Gr hybrids can enhance the valid surface of electrode (curve b). After AuNPs are deposited on $SnO_2$ NCs-Gr/GCE, the current respond further enhances (curve c) in that AuNPs are parallel to a conductor. For comparison, one same diameter gold electrode is used as working electrode (curve d), but the redox peak currents are weaker than that of AuNPs/$SnO_2$ NCs-Gr/GCE. The CV results suggest that the AuNPs/$SnO_2$ NCs-Gr reveal its favorable performance in signal amplification.

EIS is a valuable measure for researching interfacial performance of surface-modified electrodes and charge-transfer resistance at the electrode surface.

The biosensor fabrication was also evaluated by EIS (Fig. 3B). As shown in EIS, with $SnO_2$ NCs-Gr (curve b) assembled on the GCE, the charge transfer resistance ($R_{ct}$) becomes smaller than that of bare GCE (curve a) because of its good electrical conductivity. The $R_{ct}$ decreases obviously (curve c) when AuNPs are electrodeposited on the $SnO_2$ NCs-Gr/GCE. However, the $R_{ct}$ value increases observably after the modification of HP and MCH (curve d), which is due to negative charge bases of HP. When duplication–incision–replacement reaction is performed, a reduced $R_{ct}$ value is observed (curve e). The formed rigid double-stranded DNA (dsDNA) increases the negative-charged of the electrode, impeding the electron transfer. Nevertheless, revealed HP facilitates approachability of potassium ferricyanide to electrode surface which is in contrast to the looped HP with closely crowded construction, and it increases electron transfer rate [40,41]. So, the latter gets the lower $R_{ct}$ value than HP. In addition, applying SP-AuNPs on electrode increases $R_{ct}$ value (curve f). Although good conductivity of AuNPs has been proven in previous work [42], hereupon the introduction of abundant SP on AuNPs increases negative-charged of electrode. Besides, $R_{ct}$ value enlarges obviously while SA-ALP is added, which can be ascribed to this big molecule protein induces the electrostatic repulsive force between SA-ALP and $[Fe(CN)_6]^{3-/4-}$ (curve g).

DPV was used to testify the signal-amplification effect of autonomous cascade DNA duplication strategy (Fig. 3C). An obvious electrochemical oxidation signal is observed in codependence of analyte, nicking endonuclease and KF polymerase (curve d). Contrastively, in absence of target, only an extremely weak

electrochemical signal is observed (curve a), which is due to that HP can't release from its loop in condition of no target DNA, and the biotin labeled SP-AuNPs can't combine with HP. Almost the same response is acquired in existence of analyte but KF (curve b), manifesting KF polymerase acts on the target DNA and opens to reveal the part 3 for further combining of SP-AuNPs and SA-ALP. Moreover, current respond in defect of nicking endonuclease obviously reduces (curve c). In a word, the concurrence of analyted, nicking endonuclease and KF polymerase is prerequisite for the autonomous duplication–incision–replacement process.

In our detection system, AA is generated from AAP by the enzymatic reaction of ALP (equation 1). The DPV of this biosensor in different systems can explain the function of every substance in the detection system (Fig. 3D). No redox response is obtained in AAP and AAP/TCEP solution because AA induces an infirm peak current and its firsthand electrochemical oxidation demands a high anodic potential [43-45]. The existence of FcM causes an evident enhancement in anodic current (curve c) and cathodic current (curve e), indicating an electrochemical–chemical (EC) process in the system. It also suggests FcM mediates electron transfer from AA to electrode surface. Thus, the result also demonstrates that FcM is reproduced after its electrochemical oxidation by the generated AA (equations 2 and 3). Moreover, the existence of TCEP induces a substantial enhancement on peak current that ascribes to the reborn of AA (equation 4). The result indicates EC reaction is facilitated by chemical-chemical process, thereby achieving current respond amplification. Fig. 3E shows the chemical structures of AAP, FcM, TCEP and their relevant products.

$$AAP \xrightarrow{ALP} AA \quad (1)$$

$$FcM \xrightarrow{\text{Electro-oxidization}} FcM^{+} \quad (2)$$

$$FcM^{+} + AA \longrightarrow FcM + DAA \quad (3)$$

$$DAA + TCEP \longrightarrow AA + TCEP{=}O \quad (4)$$

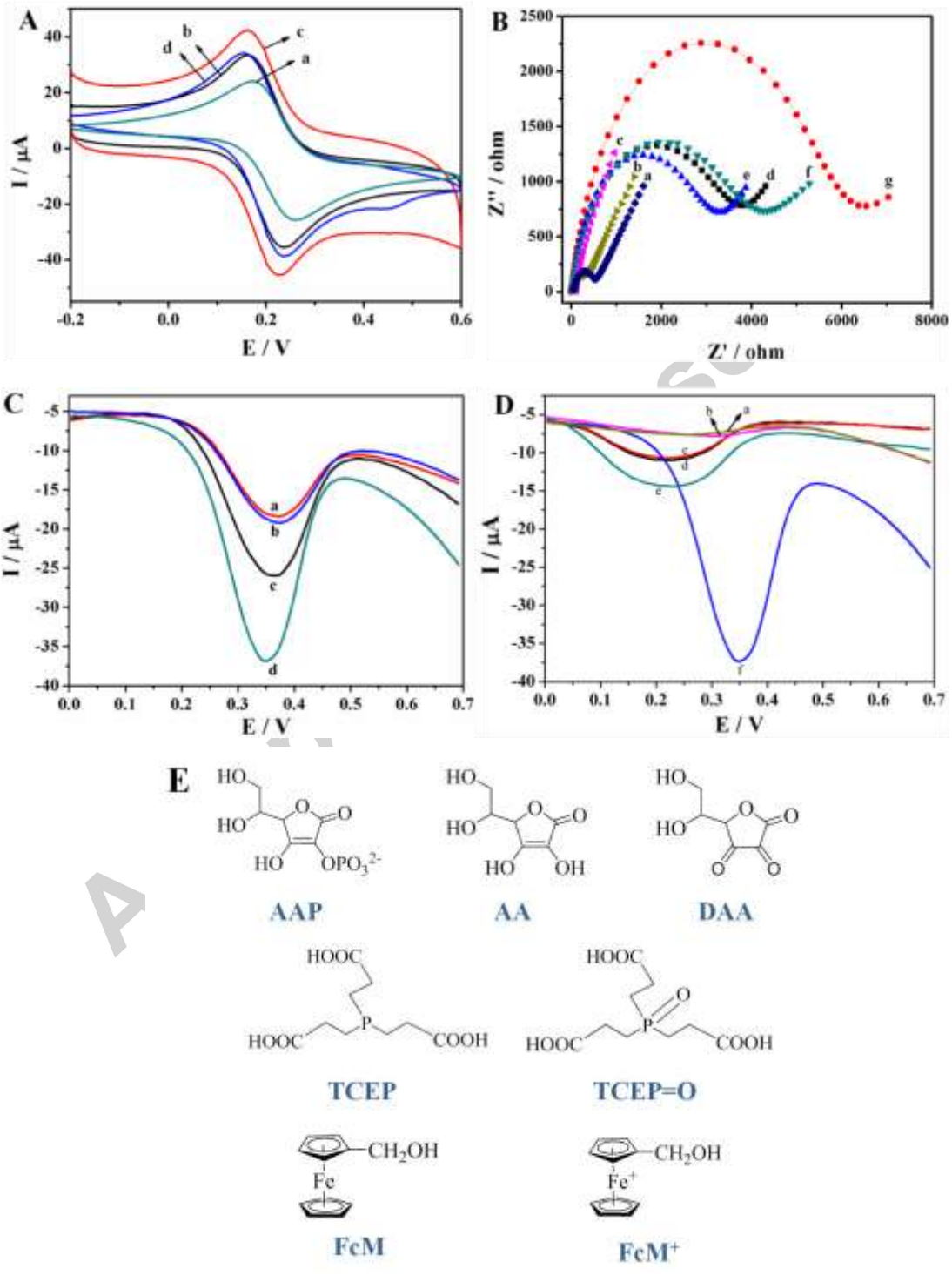

**Fig. 3** (A) CV of (a) GCE, (b) $SnO_2$ NCs-Gr/GCE, (c) AuNPs/$SnO_2$ NCs-Gr/GCE, (d) gold electrode; (B) EIS of (a) GCE, (b) $SnO_2$ NCs-Gr/GCE, (c) AuNPs/$SnO_2$ NCs-Gr/GCE, (d) HP/AuNPs/$SnO_2$ NCs-Gr/GCE, (e) TD, nicking endonuclease and KF polymerase reacted with HP/AuNPs/$SnO_2$ NCs-Gr/GCE, (f) SP-AuNPs/TD, nicking endonuclease and KF polymerase reacted with HP/AuNPs/$SnO_2$ NCs-Gr/GCE, (g) SA-ALP/SP-AuNPs/TD, nicking endonuclease and KF polymerase reacted with HP/AuNPs/$SnO_2$ NCs-Gr/GCE; (C) DPV of biosensor in solution of (a) no TD, (b) TD/nicking endonuclease (c) TD/KF polymerase and (d) TD/nicking endonuclease/KF polymerase; (D) DPV of (a) AAP, (b) AAP/TCEP (c) FcM (d) TCEP/FcM, (e) AAP/FcM and (f) AAP/TCEP/FcM. TD is 10 pM; (E) The chemical structures of AAP, FcM, TCEP and their relevant products.

### 3.5. Optimization

For achieving an optimal result, the experimental conditions were optimized. The concentration of SP DNA on the AuNPs plays a vital role. It was straightforward determined by adding various SP DNA levels in time of preparing SP-AuNPs which were obtained by mixing 1 mL AuNPs solution with 50 μL SP DNA with different concentrations (5, 10, 15 and 20 μM). It can be found from Fig. 4A that 10 μM SP DNA produces a biggest electrochemical response. The higher concentration of SP DNA gains the higher surface density on AuNPs, which is likely to limit the recognition potency of the SP-AuNPs to bind with HP due to the steric hindrance.The effect of amounts of Nb.BbvCI nicking endonuclease, KF polymerase and reaction

time were evaluated. 2, 4, 6, 8, 9, 10 units of Nb.BbvCI and KF polymerase were evaluated. The optimized amount of Nb.BbvCI nicking endonuclease is the same as KF polymerase of 8.0 Units (Fig. 4B and C). The influence of reaction time toward the autonomous DNA duplication–incision–replacement reaction on the DPV response was also studied. As shown in Fig. 4D, the peak currents obviously enhance with increasing the reaction time from 30 to 120 min, and nearly stabilized after 120 min, indicating the reaction is accomplished. Therefore, 120 min of reaction time is used.

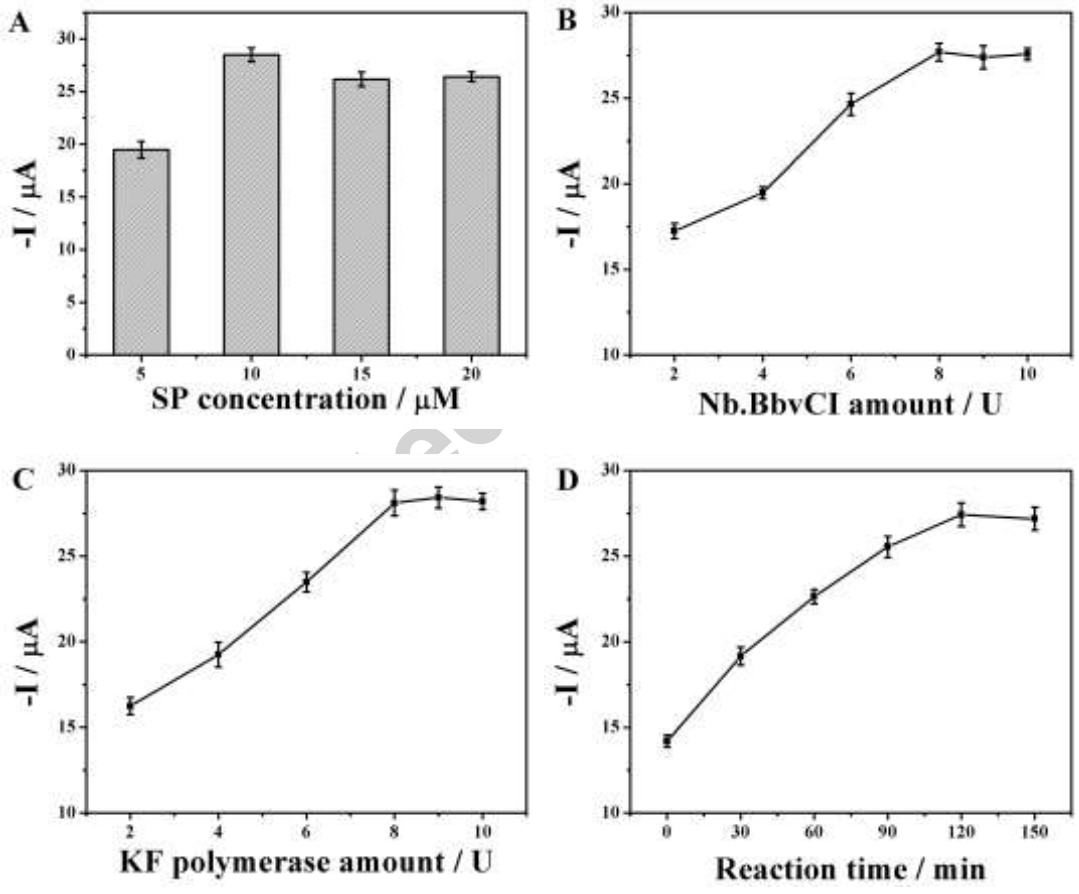


**Fig. 4** Effects of SP concentration (A), the amount of Nb.BbvCI (B) and KF polymerase (C), and reaction time (D) on the DPV response.

### 3.6. Analytical performances

Fig. 5A displays DPV respond improves with the increasing of target DNA concentration. It shows a wide linear range from 1 fM to 10 pM (the inset of Fig. 5B). The regression equation is $i$ (μA) = -4.91 log ($c$/M)-82.98 ($R$ = 0.995) and the detection limit is $1.25\times10^{-17}$ M (S/N=3). This detection limit is preferable compared most of the other DNA biosensors (Table S1).

The effect of nicking endonuclease was also studied. It indicated that the target triggered polymerization reaction could reveal HP. Fig. S1 exhibits peak current enhances with the increasing of target concentration. The linear range is 10 pM-100 nM (the inset of Fig. S1). The linear calibration equation is $i$ (μA) = -3.72 log ($c$/M)-51.58, ($R$ = 0.996). Detection limit is $1.36\times10^{-14}$ mol $L^{-1}$ (S/N=3). The results show that autonomous cascade target replication can greatly improve the analytical performance of the biosensor.

### 3.7. Selectivity, reproducibility and stability

The selectivity of proposed sensor was further studied. Complementary sequence (TD), single-base mismatched sequence (1MT), three-base mismatched sequence (3MT) and non-complementary sequence (NC) were used. As shown in Fig. 5C, the highest DPV respond is obtained when the complementary sequence is used. The peak currents of blank, NC sequence and 3MT sequence are negligible. For the single-base mismatched sequence, the peak current also is much lower than TD. The results indicate a good selectivity of the developed biosensor.

The proposed biosensor has ability to be reproduced for continuing determination target DNA. Fig. 5D shows the reproducibility dada about the biosensor. The Bar 0 denotes the original electrochemical signal of 10 pM targets. Bars 1-3 denote respond signals of reproduced HP electrode. The figure indicates that the efficient detection of target DNA can be achieved identically even though after its repetition for three times, manifesting a good reproducibility.

The stability of the DNA detection strategy was researched. The biosensor was incubated in ultrapure water, TE buffer, Tris buffer and washing buffer at 30 °C for 6 h, respectively. After that, the biosensor was exposed to target DNA and the DPV was recorded. The results manifested that the proposed biosensor almost had the identical signal as the untreated biosensor. The long-term stability of the biosensors was studied. They were kept under 4 °C for two weeks and 96.2% of the original current value was obtained, demonstrating a good stability.

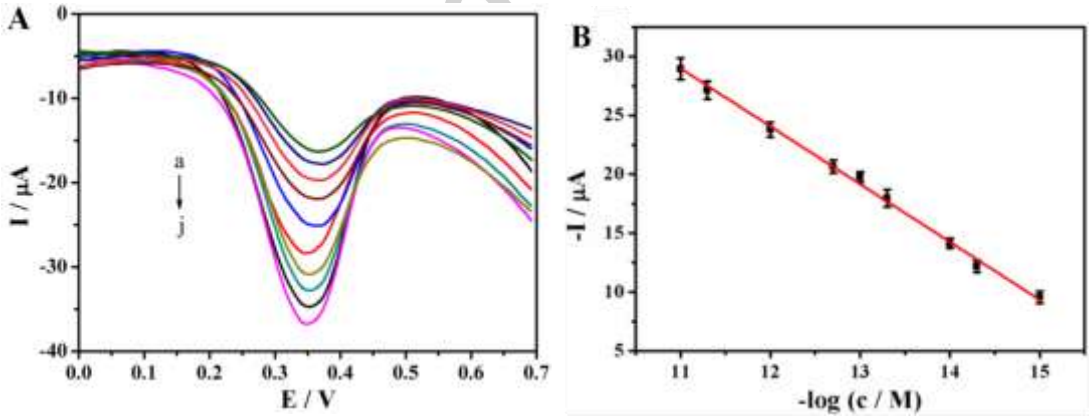

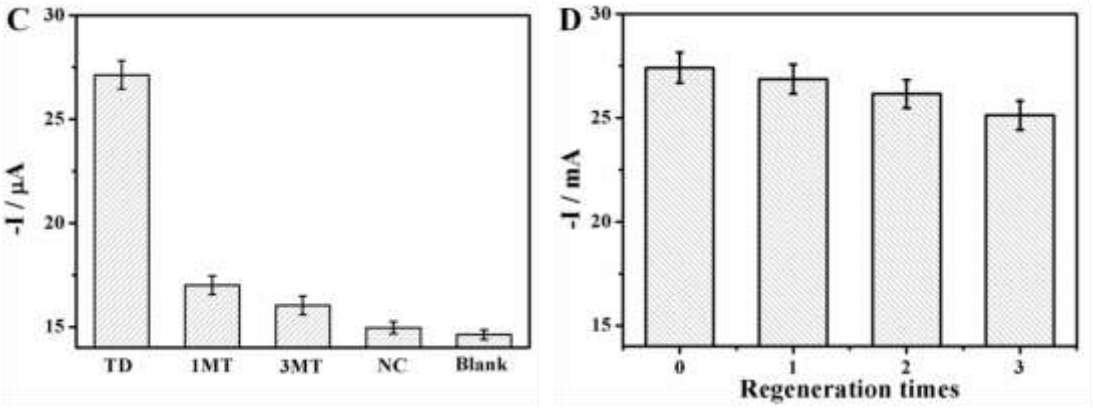


**Fig. 5** (A) DPVs of various DNA (a-j): 0, 1, 5, 10, 50, 100, 200, 1000, 5000, 10000 fM; (B) the linear relationship plots of the DPV current value versus the logarithm DNA concentration; (C) the effect of different analytes (10 pM); (D) the effect of the regeneration times.

### 3.8. Real samples detection

The proposed strategy was applied to detect target DNA in serum. Firstly, 0.1 mL serum was added in 1.0 mL PBS. Then different DNA levels (0.01, 10, 5 00 pM) were added, and the DPV response was recorded by using the biosensor. The obtained peak currents in serum (-21.7, -25.3, and -28.9 μA) were similar to that in 0.1 M PBS (-22.3, -25.9, and -29.4 μA), indicating good prospects of the developed biosensor for practical clinical diagnosis.

## 4. Conclusions

An isothermal and sensitive electrochemical DNA detection strategy based on $SnO_2$ NCs-Gr was developed by combining with autonomous cascade DNA replication. The developed biosensor had some specific merits. Firstly, the good

conductivity of $SnO_2$ NCs-Gr hybrids provided a hopeful biosensor platform; secondly, the autonomous DNA duplication–incision–replacement reaction endowed consequential signal enhancement; thirdly, SP-AuNPs afforded a continuing signal amplification for biosensor; finally, the application of EEC redox cycling leaded to a remarkable lower detection limit (0.0125 fM). The fabricated sensor was easily reproduced and therefore held great potential in biological analysis.

## Acknowledgments

This work was supported by the National Natural Science Foundation of China (21475115), Program for University Innovative Research Team of Henan (15IRTSTHN001), Henan Provincial Science and technology innovation team (C20150026), Nanhu Scholars Program of XYNU and Henan Science and Technology Cooperation Project (172106000064).

## References

[1] H.Y. Zhu, M.J. Zhang, L. Zou, R.M. Li, L.S. Ling, Talanta, 173 (2017) 9-13.

[2] Z. Taleat, M.M. Ardakani, H. Naeimi, H. Beitollahi, M. Nejati, H.R. Zare, Anal. Sci. 24 (2008) 1039-1044.

[3] H. Beitollahi, H. Karimi-Maleh, H. Khabazzadeh, Anal. Chem. 80 (2008) 9848–9851.

[4] M. Mazloum-Ardakani, B. Ganjipour, H. Beitollahi, M.K. Amini, F. Mirkhalaf, H. Naeimi, M. Nejati-Barzoki, Electrochimica Acta, 2011, 56(25):9113-9120.

[5] M.M. Foroughi, H. Beitollahi, S. Tajik, M. Hamzavi, H. Parvan, Int. J. Electrochem. Sci. 9 (2014) 2955-2965.

[6] S. Mohammadi, H. Beitollahi, A. Mohadesi, Sensor Lett. 11 (2013) 388-394.

[7] H. Beitollahi, M.A. Taher, M. Ahmadipour, R. Hosseinzadeh, Measurement 47 (2014) 770-776.

[8] K.J. Huang, H.L. Shuai, J.Z. Zhang, Biosens. Bioelectron. 77 (2016) 69-75.

[9] K. Tanaka, M. Iwashita, M. Matsushima, Y. Wachi, T. Izawa, K. Sakai, Y. Kobayashi, J. Matern.-Fetal Neonatal Med. 29 (2016) 130-134.

[10] L.L. Hao, H.J. Gu, N. Duan, S.J. Wu, X.Y. Ma, Y. Xia, H.T. Wang, Z.P. Wang, Talanta 164 (2017) 275-282.

[11] H.Y. Xu, Q.W. Wu, H. Shen, Talanta 167 (2017) 630-637.

[12] Y. Shen, D.J. Rao, W.S. Bai, Q.L. Sheng, J.B. Zheng, Talanta 165 (2017) 304-312.

[13] R.G. Shi, J. Liang, Z.S. Zhao, A.F. Liu, Y. Tian, Talanta 169 (2017) 37-43.

[14] Y.J. Song, K.G. Qu, C. Zhao, J.S. Ren, X.G. Qu, Adv. Mater. 22 (2010) 2206-2210.

[15] F.W. Zeng, Z.H. Sun, X.G. Sang, D. Diamond, K.T. Lau, X.X. Liu, D.S. Su, Chemsuschem 4 (2011) 1587-1591.

[16] J. Han, L. Jiang, F. Li, P. Wang, Q. Liu, Y.H. Dong, Y.Y. Li, Q. Wei, Biosens. Bioelectro. 77 (2016) 1104-1111.

[17] B. Quan, W. Liu, Y.S. Liu, Y. Zheng, G.C. Yang, G.B. Ji, J. Colloid and Interf. Sci. 481 (2016) 13-19.

[18] K.N. Zhao, L. Zhang, R. Xia, Y.F. Dong, W.W. Xu, C.J. Niu, L. He, M.Y. Yan, L.B. Qu, L.Q. Mai, Small 12 (2016) 588-594.

[19] M. Yuasa, K. Suematsu, K. Yamada, K. Watanabe, T. Kida, N. Yamazoe, K. Shimanoe, Crystal Growth & Design 16 (2016) 4203-4208.

[20] G.Q. Zhang, X.W. Lou, Adv. Mater. 25 (2013) 976-979.

[21] R.Z. Ma, T. Sasaki, Adv. Mater. 22 (2010) 5082-5104.

[22] Z. Zhang, R. Zou, G. Song, L. Yu, Z. Chen, J. Hu, J. Mater. Chem. 21 (2011) 17360-17365.

[23] S. F. Liu, W.J. Wei, Y.Q. Wang, L. Fang, L. Wang, F. Li, Biosens. Bioelectron. 80 (2016) 208-214.

[24] L. Freage, F. Wang, R. Orbach, I. Willner, Anal. Chem. 86 (2014) 11326-11333.

[25] A. Chen, G. Gui, Y. Zhuo, Y. Chai, Y. Xiang, R. Yuan, Anal. Chem. 87 (2015) 6328-6334.

[26] W. S. Hummers, R. E. Offeman, J. Am. Chem. Soc. 80 (1958) 1339-1339.

[27] K.J. Huang, Y.J. Liu, H.B. Wang, Y.Y. Wang, Y.M. Liu, Biosens. Bioelectron. 55 (2014) 195-202.

[28] Y. Li, X.D. Qi, C.C. Lei, Q.F. Yue, S.S. Zhang, Chem. Commun. 50 (2014) 9907-9909.

[29] J. Van Ness, L.K. Van Ness, D.J. Galas, Proc. Nat. Acad. Sci. 100 (2003) 4504-4509.

[30] H. Jia, Z. Li, C. Liu, Y. Cheng, Angew. Chem. Int. 49 (2010) 5498-5501.

[31] M.R. Akanda, M.A. Aziz, K. Jo, V. Tamilavan, M.H. Hyun, S. Kim, H. Yang, Anal. Chem. 83 (2011) 3926-3933.

[32] L. Zhang, R. Miranda-Castro, C. Stines-Chaumeil, N. Mano, G. Xu, F. Mavré, B. Limoges, Anal. Chem. 86 (2014) 2257-2267.

[33] L. Liu, Y.P. Gao, H.P. Liu, J.M. Du, N. Xia, Electrochim. Acta 139 (2014) 323-330.

[34] N. Xia, L. Liu, R.J. Wu, H.P. Liu, S.J. Li, Y.Q. Hao, J. Electroanal. Chem. 731 (2014) 78-83.

[35] L. Vayssieres, M. Graetzel, Angew. Chem. Int. Ed. 43 (2004) 3752-3756.

[36] H.J. Song, L.C. Zhang, C.L. He, Y. Qu, Y.F. Tian, Y. Lv, J. Mater. Chem. 21 (2011) 5972-5977.

[37] X. Yao, G.L. Guo, X. Ma, Y. Zhao, C.Y. Ang, Z. Luo, K.T. Nguyen, P.Z. Li, Q.Y. Yan, Y.L. Zhao, ACS Appl. Mater. Interf. 47 (2015) 26085-26093.

[38] W.J. Wang, J.J. Li, K. Rui, P.P. Gai, J.R. Zhang, J.J. Zhu, Anal. Chem. 87 (2015) 3019-3026.

[39] Z. Wang, N. Sun, Y. He, Y. Liu, J. Li, Anal. Chem. 86 (2014) 6153-6159.

[40] N. Yang, Y. Cao, P. Han, X. Zhu, X. Sun, G. Li, Anal. Chem. 84 (2012) 2492-2497.

[41] S. Liu, C. Wang, C. Zhang, Y. Wang, B. Tang, Anal. Chem. 85 (2013) 2282-2288.

[42] X.L. Luo, J.J. Xu, G.J. Yang, H.Y. Chen, Biosens. Bioelectro. 21 (2005) 190-196.

[43] D. Du, J. Wang, L.M. Wang, D.L. Lu, Y.H. Lin, Anal. Chem. 84 (2012)

1380-1385.

[44] G.D. Liu, S.L. Riechers, M.C. Mellen, Y.H. Lin, Electrochem. Commun. 7 (2005) 1163-1169.

[45] N. Xia, Y.J. Zhang, X. Wei, Y.P. Huang, L. Lin, Anal. Chim. Acta. 878 (2015) 95-101.

## Highlights

- Stannic oxide nanocorals-graphene hybrids were prepared by a facile hydrothermal method.
- An autonomous cascade DNA replication strategy was applied for signal amplification.
- An electrochemical-chemical-chemical redox cycling system was used.
- The biosensor shows a detection limit of 0.0125 fM and high specificity towards target DNA.